Pferdeheilkunde – Equine Medicine 39 (2023) 2 (March/April) 158–167 DOI 10.21836/PEM20230205

Ex vivo validation of delayed gadolinium-enhanced magnetic resonance imaging (MRI) of cartilage (dGEMRIC) and T2 mapping for quantifying cartilage thickness in normal and naturally occurred osteoarthritic distal interphalangeal joints using a high-field MRI

Andrea S. Bischofberger[1], Regula Fürst[2], Anton Fürst[2], Monika Hilbe[3], Paul R. Torgerson[4] and Patrick Kircher[1]

[1] Division of Diagnostic Imaging, Vetsuisse-Faculty, University of Zürich
[2] Equine Hospital, Vetsuisse-Faculty, University of Zürich
[3] Institute of Veterinary Pathology, Vetsuisse-Faculty, University of Zürich
[4] Section of Veterinary Epidemiology, Vetsuisse-Faculty, University of Zürich

Summary: Determination of measurements of cartilage thickness on dGEMRIC, T2 maps and histology of pre-determined sites in normal and naturally occurring osteoarthritic Warmblood cadaver distal interphalangeal joints (DIPJs), correlation of histological and MRI measurements, and testing of the effect of cartilage health and cartilage position within the joint on the cartilage thickness (histological and MRI measurements). From 12 Warmblood DIPJ cadavers cartilage thickness was obtained from dGEMRIC images after intra-articular gadolinium administration ($T1_{postGd}$) and from $T2_{maps}$ using a 3 tesla magnet at predetermined sites in the DIPJ. Corresponding cartilage sites underwent histologic evaluation to determine cartilage health and cartilage thickness was measured by 2 observers. Interobserver agreement was calculated using intraclass correlation coefficients. Mean $T1_{postGd}$ and $T2_{map}$ cartilage thickness was correlated with histological cartilage thickness. Mixed generalised linear models were created to evaluate the effects of cartilage site, articular surface, and cartilage health on cartilage thickness. 122 cartilage specimens were analysed. $T1_{postGd}$ ($r = 0.42–0.43$; $P < 0.001$) and $T2_{map}$ ($r = 0.34–0.35$; $P < 0.001$) cartilage thickness correlated positively with histological cartilage thickness. $T1_{postGd}$ cartilage thickness significantly decreased as osteoarthritis progressed. There were topical variations in cartilage thickness. Whereby articular cartilage was thinnest situated in the dorsal DIPJ zone ($T1_{PostGd}$, $T2_{map}$ and histology), on the condyles ($T2_{map}$) and on the distal aspect of the middle phalanx (histology). In conclusion $T1_{PostGd}$ and $T2_{map}$ are reliable to evaluate the thickness of normal and osteoarthritic equine articular cartilage, whereby $T1_{PostGd}$ is superior. Topographical variations of DIPJ cartilage thickness should be appreciated by clinicians to avoid misinterpretation of cartilage thinning secondary to cartilage disease. Volume averaging should be appreciated as a complicating factor, especially in the joint periphery.

Keywords: cartilage, delayed gadolinium-enhanced magnetic resonance imaging of cartilage, dGEMRIC, , T2 mapping, horse, MRI, osteoarthritis, distal interphalangeal joint

Citation: Bischofberger A. S., Fürst R., Fürst A., Hilbe M., Torgerson P. R., Kircher P. (2023) Ex-vivo validation of delayed gadolinium-enhanced magnetic resonance imaging (MRI) of cartilage (dGEMRIC) and T2 mapping for quantifying cartilage thickness in normal and naturally occurred osteoarthritic distal interphalangeal joints using a high-field MRI. Pferdeheilkunde 39, 158–167; DOI 10.21836/PEM20230205

Correspondence: PD Dr. med. vet. Andrea Bischofberger PhD, DACVS/ECVS, Division of Diagnostic Imaging, Department of Clinical Services, Vetsuisse-Faculty, University of Zürich, Winterthurerstrasse 260, 8057 Zürich, Switzerland; abischofberger@vetclinics.uzh.ch

Submitted: January 18, 2023 | **Accepted:** February 16, 2023

Introduction

Naturally occurring osteoarthritis (OA) is one of the key reasons for wastage in horses (*Jeffcott* et al. 1982). Each joint can be affected by OA and there are often multiple joints affected in one horse simultaneously. Depending on the breed, the age, and the use of the horse individual joints may be affected more often than others. The distal interphalangeal joint (DIPJ) for example, is a common site for OA in sport horses (*Dyson* 1991, *Kristiansen* et al. 2007, *McKnight* 2012).

OA is a degenerative disease, characterized by the proteolytic breakdown of the cartilage matrix, fibrillation and erosion of the cartilage surface, and the release of breakdown products resulting in synovitis (*Goodrich* et al. 2006, *Frisbie* 2012). Early articular cartilage lesions may not show signs of pain due to the lack of nociceptive receptors in this type of tissue. This implies that cartilage damage can and does progress, while no clinical signs such as lameness are yet apparent (*Bekkers* et al. 2010, *Pease* 2012). It is therefore imperative to detect cartilage injury early, enabling pathologic conditions to be addressed, before they have progressed, and allowing timely therapy to be implemented.

Conventional magnetic resonance imaging (MRI) methods have shown morphological articular cartilage changes based

on imaging the tissue's hydrogen content (*Nelson* et al. 2021). However, morphological cartilage changes are preceded by biochemical and structural changes, which can be evaluated by cartilage imaging techniques such as delayed gadolinium enhanced magnetic resonance imaging of cartilage (dGEMRIC) and T2 cartilage mapping (*Domayer* et al. 2008). In humans such MRI techniques have rapidly developed in recent years and have been used to identify early stages of OA (*Trattnig* et al. 1999, *Gold* et al. 2006, *Trattnig* et al. 2007, *Trattnig* et al. 2008, *Potter* et al. 2009, *Bekkers* et al. 2013).

Gadolinium diethylene triamine pentaacetic acid (Gd-DPTA^{2}-) is injected either intraarticularly or intravenously, permeates the hyaline cartilage and disperses in an inverse relationship to the articular cartilage proteoglycan content. In areas of cartilage degeneration, the Gd-DPTA^{2}- uptake increases as a result of the relative decrease in negative charge of the proteoglycan-depleted cartilage. By post-processing the images and producing relaxation time color maps, a visual representation of the cartilage relaxation times is obtained (*Choi* et al. 2011, *Pease* 2012).

Collagen fibers are organised to maximise the efficiency in the transmission of joint forces and joint lubrication. Loss of this orientation is a hallmark feature of OA (*Goodwin* 2001, *Xia* et al. 2002). Early degenerative changes in the extracellular matrix increase the overall water content via osmosis and the water mobility. T2 cartilage mapping ($T2_{map}$) is sensitive for determining the collagen amount, the collagen orientation and the water content in the articular cartilage (*Mosher* and *Dardzinski* 2004).

Only a handful of reports on dGEMRIC and T2 cartilage mapping have been reported in horses (*Menendez* et al. 2011, *Carstens* et al. 2013, *Carstens* et al. 2013, *Bischofberger* et al. 2018, *Baker* et al. 2022). To ensure that the bone-cartilage interface and the cartilage surface of the dGEMRIC and T2 mapping sites are consistent with true anatomical areas, validation studies comparing MRI to histological measurements as the reference are needed before the cartilage boundaries can be accurately identified and the cartilage itself can be reliably evaluated. This is especially true for a complex joint like the DIPJ.

Different studies have measured the cartilage thickness or the joint space width by MRI in different equine joints (*Olive* et al. 2010, *Carstens* et al. 2013). Cartilage thickness of 20 Thoroughbred metacarpophalangeal joints was measured on MRI and histology. The study illustrated that MRI allows clinically applicable, satisfactory assessment of the articular cartilage thickness, the structure and to a lesser extent, early biochemical alterations in the osteoarthritic joint (*Olive* et al. 2010). dGEMRIC and T2 mapping were found to be accurate techniques for measuring the distal third metacarpal/metatarsal bone cartilage thickness at locations, where the cartilage was not in direct contact with the proximal phalanx cartilage. The thin distal third metacarpal/metatarsal bone cartilage and the limit of detection of the measuring device, were however the main limitations in this study (*Carstens* et al. 2013).

The objectives of the study reported here were 1) to determine measurements of cartilage thickness on dGEMRIC, T2 maps and histology of pre-determined sites in normal and naturally occurring osteoarthritic Warmblood cadaver DIPJs, and 2) to correlate histological and MRI measurements, and to test the effect of cartilage health and cartilage location within the joint on the cartilage thickness (histological and MR measurements). We hypothesized that 1) there would be a good correlation between MRI and histological measurements, and that 2) osteoarthritic cartilage would be thinner than normal cartilage, and that there would be site dependent differences in cartilage thickness within the DIPJ.

Material and methods

Sample

From 12 Warmblood horses (mean ± standard deviation age, 15.2 ± 9.2 years; range, (6–32 years)), euthanised for reasons unrelated to the musculoskeletal apparatus and following owner consent, the distal aspect of the left or right forelimb was harvested. The limbs were removed from the body at the level of the middle carpal joint and stored at 4 °C until scanned.

MRI

Each DIPJ was scanned within 24 hours following harvest at room temperature (approximately 22 °C) on 12 different days over a 4-month period. Each DIPJ was positioned with the dorsal hoof wall facing downward and the toe facing toward the gantry using a 16-channel knee coil and a 3-tesla MRI scanner (Phillips Health Care Ingenia, Phillips AG, Zürich, Switzerland). A frontal localiser was run to identify the condylar and intercondylar sagittal slices for each DIPJ. $T1_{preGd}$ was measured with single slice inversion recovery spin echo sequences (Repetition time (TR) 12 ms, echo time (TE) 5.6 ms, field of view 100 × 100 mm, matrix 252 × 244, slice thickness 3 mm, receiver band width 131.6 kHz/pixel) for each lateral and medial mid condylar sagittal slice and the central inter condylar sagittal slice (positioned in the middle of the distal aspect of the middle phalanx (P2) sagittal groove). T2 maps were obtained using multi-slice, multi-echo, spin-echo sequences (TR 2000 ms, TE 6 × 13 ms, field of view 160 × 160 mm, matrix 380 × 311, slice thickness 2.5 mm, receiver band width 291.1 kHz/pixel). By placing a 21-gauge needle into the dorsal recess of the DIPJ, as much synovial fluid as possible was aspirated to minimise the dilution of Gd-DTPA^{2}-, and to minimise fluid-related sources of variability. Then, 0.05 ml Gd-DTPA^{2}- (Magnevist gadopentate dimeglumine, Bayer Health Care Pharmaceuticals, Zürich, Switzerland) diluted in 5 ml 0.9 % NaCl solution was injected into the DIPJ (Gd-DTPA^{2-} dose, 0.025 mmol/joint). The limbs were manually flexed for 5 minutes to distribute the Gd-DTPA^{2}- within the joint. Two hours after the Gd-DTPA^{2}- injection the limbs were scanned again and the $T1_{postGd}$ was measured on the mid condylar and central intercondylar sagittal slices analogue to the $T1_{preGd}$.

Tissue harvesting and histological processing

The DIPJs were disarticulated and osteochondral cores (8 mm diameter) were cut from distal P2 (Figure 1A) and proximal

distal phalanx (P3) (Figure 1B) using an OATS (osteochondral autograft transfer system) cutting tube (Arthrex Inc, Naples, FL, USA). A total of eleven cores were obtained per joint. A central 1000μm thick osteochondral slice was cut from the core using a saw and further processed for histological sections. Briefly the osteochondral samples were fixed in 4% paraformaldehyde for 48 hours, decalcified in 25% EDTA for 4 weeks, embedded in paraffin and sections were cut and stained with haematoxylin and eosin, Safranin-O-Fast green and toluidine blue.

Histological analysis

Safranin-O-Fast green stained sections were analysed and scored for degenerative changes by 3 blinded observers (3 veterinarians supervised by a European specialist pathologist) using a modified *Mankin* scoring system (Table 1) (*Mankin* et al. 1971, *Lacourt* et al. 2012). The histological sections of the different sites were scored on the basis of the criteria shown in Table 1. According to the overall mean *Mankin* score 3 groups of cartilage health were made: normal cartilage: *Mankin* score = 0–1.9; minimal to moderate OA: *Mankin* score = 2.0–8.0; severe OA: *Mankin* score = 8.1–16.0.

Two observers obtained the measurements as described in Fig. 2 with a 1-month interval. A Leica DM LB2 light microscope equipped with a Leica DC 480 camera was used (Leica Microsystems Ltd, Heerbrugg, Switzerland). Total cartilage (TC) and hyaline cartilage (HC) thickness (Figure 2) were each measured 3 times. When measuring the HC the TC is excluded from the measurement as shown in Figure 2. The mean ± standard deviation of the 3 measurements of each observer was calculated and used for further analysis.

MRI analysis

All sites (defined as shown in Figure 1, 3) were analysed for each mid condylar and the central inter condylar $T1_{postGd}$ scan and $T2_{map}$. Three sites were analysed for each mid condylar and the inter condylar sagittal slice (Figure 3). The locations of those measurements were standardised. The MR image was zoomed into an optimal position, where a translucent overlay template (as shown in Figure 3) determined the center point in the middle of the condyles of P2 and the midline that ran vertically through the DIPJ. The optimal window was found by using the windowing tool in the software and the sites were defined, where the cartilage, the joint space and the surface of the bone could best be identified. Cartilage thickness was measured using a commercially available measuring software (Osirix MD Version 7.5, Bernex, Switzerland). Two observers blinded to cartilage health status measured cartilage thickness at each site 3 times and the mean ± standard deviation of each site of each observer was calculated. The second observer undertook the measurements 1 month later, but with the same settings.

Statistical analysis

The database was established in Microsoft Excel. The different sites were grouped into cartilage zones depending on their location in the joint: condyle (sites 1, 2, 3, 4, 5, 6, 7, 11) or condylar groove (sites 8, 9, 10), and dorsal zone (sites 1, 4, 8), central zone (sites 2, 5, 7, 9, 11) or palmar zone (sites 3, 6, 10).

The inter observer agreement of the cartilage thickness measurements (histological and MRI) and the mean overall car-

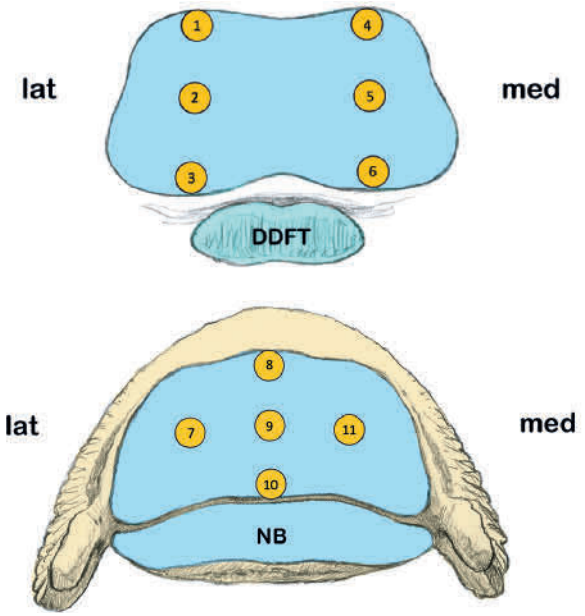

Fig. 1 Schematic drawing of the distal aspect of the middle phalanx (P2) (A) and proximal aspect of the distal phalanx (P3) (B) hyaline cartilage surface, showing the locations of the obtained core biopsies for histological and MR image analyses. (lat = lateral; med = medial, NB = navicular bone, DDFT = deep digital flexor tendon.). | *Schematische Darstellung des distalen Aspekts der mittleren Phalanx (P2) (A) und des proximalen Aspekts der distalen Phalanx (P3) (B) der hyalinen Knorpeloberfläche mit Angabe der Stellen, an denen die Kernbiopsien für die histologische und MR-Bildanalyse entnommen wurden. (lat = lateral; med = medial, NB = Strahlbein, DDFT = tiefe Beugesehne).*

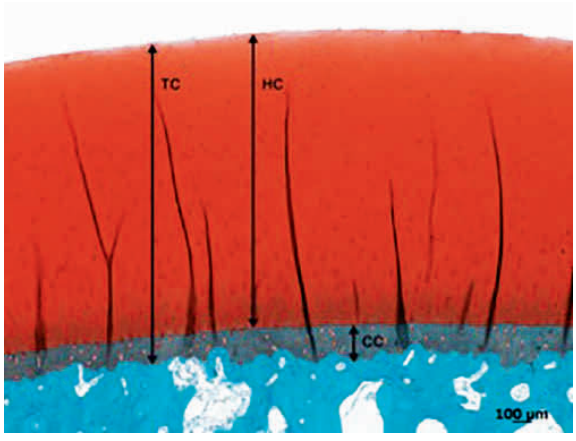

Fig. 2 Safranin-O Fast Green stain of a core biopsy obtained from the DIPJ showing normal cartilage and the indicated cartilage thickness measurements. TC: total cartilage thickness, HC: hyaline cartilage thickness, CC: calcified cartilage thickness. | *Safranin-O Fast Green-Färbung einer aus dem Hufgelenk entnommenen Kernbiopsie mit normalem Knorpel und den angegebenen Knorpeldickenmessungen. TC: Gesamtknorpeldicke, HC: Dicke des hyalinen Knorpels, CC: Dicke des kalzifizierten Knorpels.*

tilage *Mankin* scores were analysed using intraclass correlation coefficients (ICCs). Average measures were reported and ICCs > 0.7 were considered good, > 0.8 optimal and > 0.9 excellent.

Of all observers an overall mean *Mankin* score, and an overall mean $T1_{PostGd}$ and $T2_{map}$ cartilage thickness measurement were calculated, and included in the further analyses. A Kolmogorov-Smirnoff Test of normality was used to evaluate the distribution of the data. Results of parametric data were displayed as mean ± standard deviation and results of non-parametric data were displayed as median (range). Associations between the mean histological cartilage thickness measurements (TC, HC) and the MRI cartilage thickness measurements $T1_{PostGd}$ and $T2_{map}$ were investigated using Spearmans rho non-parametric correlations.

A mixed generalised linear model approach was used to analyse the relationship between each dependent ($T1_{PostGd}$, $T2_{map}$, TC and HC cartilage thickness) or outcome variable of interest.

Table 1 Modified Mankin scoring system that was used to histologically evaluate the core tissue samples obtained from the sites of the distal interphalangeal joint harvested from horses with and without naturally occurring osteoarthritis. | *Modifiziertes Mankin-Scoring-System, das zur histologischen Beurteilung von Gewebeproben aus dem Hufgelenk von Pferden mit und ohne natürlich auftretende Arthrose verwendet wurde.*

Score	Structure
0	Normal
1	Fibrillation
2	Fissures
3	Erosion of 1/3 of depth of the hyaline cartilage
4	Erosion of 2/3 of depth of the hyaline cartilage
5	Full depth erosion of the hyaline cartilage
6	Full depth erosion of the hyaline and calcified cartilage
	Chondrocyte density
0	No decrease in cells
1	Focal decrease in cells
2	Multifocal decrease in cells
3	Multifocal confluent decrease in cells
4	Diffuse decrease in cells
	Cluster formation
0	Normal
1	< 4 clusters
2	≥ 4 but < 8 clusters
3	≥ 8 clusters
	Safranin-O-Fast green staining
0	Uniform staining throughout articular cartilage
1	Loss of staining in the superficial zone of hyaline cartilage
2	Loss of staining in the upper 2/3 of hyaline cartilage
3	Loss of staining in all of hyaline cartilage

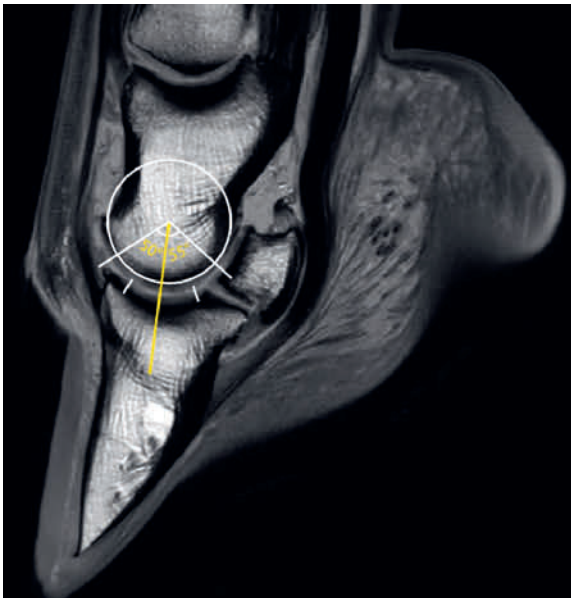

Fig. 3 Sagittal intercondylar MR image (T2 TSE cal) of the distal interphalangeal joint (DIPJ) showing a translucent template illustrating a circle placed "at best fit" over the distal aspect of the middle phalanx (P2) condyle and a yellow line drawn down the axis of the metaphysis of P2 running through the center of rotation of the DIPJ. Dorsal sites of distal aspect of P2 (sites 1, 4 – Figure 1) were defined using a 50° angle dorsal from the line drawn down the axis of the P2 metaphysis. At these dorsal sites there was no contact between the distal aspect of P2 and proximal aspect of P3 hyaline cartilage, when the joint was in a neutral position. Central sites of distal P2 (sites 2, 5 – Figure 1) were defined as the distal aspect of the line drawn down the axis of the P2 metaphysis. Palmar sites of distal aspect of P2 (sites 3, 6 – Figure 1) were defined using a 55° angle palmar from the line drawn down the axis of the P2 metaphysis. At these palmar sites there was contact between the distal aspect of P2 and the navicular bone cartilage. The dorsal site of proximal aspect of the distal phalanx (P3) (site 8) was defined as the site extending 10° palmar from the most dorsal extent of the hyaline cartilage. Central sites of proximal aspect of P3 (sites 7, 9, 11 - Figure 1) were defined as the line drawn down the axis of the P2 metaphysis. The palmar site of the proximal aspect of P3 (site 10 - Figure 1) was defined as the site extending 10° dorsally from the most palmar extent of the proximal aspect of P3 cartilage articulating with distal aspect of P2. | *Sagittale interkondyläre MR-Aufnahme (T2 TSE cal) des Hufgelenks mit einer transluzenten Schablone, die einen Kreis zeigt, der „bei bester Passung" über dem distalen Aspekt des Kondylus der Mittelphalanx (P2) platziert ist, und einer gelben Linie, die entlang der Achse der Metaphyse von P2 durch das Rotationszentrum des Hufgelenks verläuft. Die dorsalen Stellen des distalen Aspekts von P2 (Stellen 1, 4 - Abbildung 1) wurden unter einem Winkel von 50° dorsal der in der Achse der P2-Metaphyse gezogenen Linie definiert. An diesen dorsalen Stellen gab es keinen Kontakt zwischen dem distalen Aspekt von P2 und dem proximalen Aspekt des hyalinen Knorpels von P3, wenn sich das Gelenk in einer neutralen Position befand. Die zentralen Stellen des distalen P2 (Stellen 2, 5 - Abbildung 1) wurden als der distale Aspekt der entlang der Achse der P2-Metaphyse gezogenen Linie definiert. Palmar gelegene Stellen des distalen Aspekts von P2 (Stellen 3, 6 - Abbildung 1) wurden unter einem Winkel von 55° palmar von der entlang der Achse der P2-Metaphyse gezogenen Linie definiert. An diesen palmaren Stellen bestand ein Kontakt zwischen dem distalen Aspekt von P2 und dem Strahlbeinknorpel. Die dorsale Stelle des proximalen Aspekts der distalen Phalanx (P3) (Stelle 8) wurde als die Stelle definiert, die sich 10° palmar von der dorsalsten Ausdehnung des hyalinen Knorpels erstreckt. Die zentralen Stellen des proximalen Aspekts von P3 (Stellen 7, 9, 11 - Abbildung 1) wurden als die entlang der Achse der Metaphyse P2 gezogene Linie definiert. Die palmar gelegene Stelle des proximalen Aspekts von P3 (Stelle 10 - Abbildung 1) wurde als die Stelle definiert, die sich 10° dorsal von der palmaren Ausdehnung des proximalen Aspekts des P3-Knorpels erstreckt, der mit dem distalen Aspekt von P2 artikuliert.*

Independent variables evaluated as fixed effects in the respective models included bone (P2/P3), cartilage zones (condyle/condylar groove) and (dorsal/central/palmar), and cartilage health (none/mild-moderate/severe OA). Random effects for limb and replicate were included in both models to account for repeated measure within joints. Results of exploratory analysis indicated that the use of a gamma distribution to model the dependent variable provided the best fit for the data. Independent variables with $P > 0.2$ were omitted from the final model. The significance level was set at $P < 0.05$ and the analyses were undertaken in SPSS 21.0 (BM SPSS, Armonk, NY, USA) and in R (R Core Team (2016). R: A language and environment for statistical computing. R Foundation for Statistical Computing, Vienna, Austria. URL https://www.R-project.org/. using the MASS, car, and lme4 packages).

Results

Of the 132 osteochondral core tissue specimens collected from 12 DIPJs, 10 were lost during the processing. This resulted in tissue specimens of 122 sites being included in the study. There were 40 sites classified as normal articular cartilage, 68 sites as mild to moderate naturally occurring OA and 14 sites with severe naturally occurring OA.

Intraclass correlation coefficients

The inter observer agreement for the histological scoring was excellent (ICC = 0.98). The median (range) of the MRI ($T1_{PostGd}$ and $T2_{map}$) and histological cartilage thickness measurements (TC and HC) displayed by cartilage health, bone (P2/P3) and cartilage zone within the joint ((condyle/condylar groove) (dorsal/central/palmar)) are shown in Table 2. The inter observer agreement of the MRI cartilage thickness measurements was excellent (ICC = 0.953) for the $T1_{postGd}$ and optimal (ICC = 0.835) for the $T2_{map}$. The inter observer agreement of the histological cartilage thickness measurements were excellent for the TC (ICC = 0.922) and the HC (ICC = 0.939).

Correlations between MRI and histological cartilage thickness

There was a significant moderate positive correlation for $T1_{postGd}$ cartilage thickness measurements with TC ($r = 0.43$; $P < 0.001$), and with HC ($r = 0.42$; $P < 0.001$). The same was true for the $T2_{map}$ cartilage thickness measurements with TC ($r = 0.35$; $P < 0.001$) and HC ($r = 0.34$; $P < 0.001$). However, overall $T1_{postGd}$ showed greater correlation coefficients for all cartilage thickness measurements compared to $T2_{map}$. For both $T1_{postGd}$ and $T2_{map}$ the correlation coefficients (r) were similar for TC (0.43 and 0.35, respectively) and for HC thickness measurements (0.42 and 0.34, respectively).

Generalised linear mixed models

The detailed results of the generalised linear mixed models are shown in Table 2. Briefly, cartilage health had no significant effect on histological cartilage thickness measurements (TC and HC) or on $T2_{map}$. However the $T1_{postGd}$ cartilage thickness was significantly less in sites with severe OA compared to normal cartilage sites (Table 2).

Histologically measured TC and HC thicknesses in the dorsal zone were significantly less than in the central zone. However,

Table 2 Median (range) of $T1_{PostGd}$, $T2_{map}$, and histological (TC, HC) cartilage thickness measurements (μm) and the P-values of the independent parameters analysed in the 5 individual generalised linear mixed models. Significant P-values of the generalised linear mixed models are marked in bold. The sagittal cartilage zones were omitted from the model due to $P > 0.2$ when $T1_{PostGd}$ was the dependent variable. Cartilage health and bone were omitted from the final model due to $P > 0.2$ when $T2_{map}$ was the dependent variable. Cartilage health and sagittal cartilage zones were omitted from the final model due to $P > 0.2$ when HC and TC were the dependent variables. | *Median (Bereich) der $T1_{PostGd}$-, $T2_{map}$- und histologischen (TC, HC) Knorpeldickenmessungen (μm) und die P-Werte der unabhängigen Parameter, die in den 5 einzelnen verallgemeinerten linearen Mischmodellen analysiert wurden. Signifikante P-Werte der verallgemeinerten linearen gemischten Modelle sind fett markiert. Die sagittalen Knorpelzonen wurden aufgrund von $P > 0,2$ aus dem Modell ausgelassen, wenn $T1_{PostGd}$ die abhängige Variable war. Knorpelgesundheit und Knochen wurden aufgrund von $P > 0,2$ aus dem endgültigen Modell ausgeschlossen, wenn $T2_{map}$ die abhängige Variable war. Knorpelgesundheit und sagittale Knorpelzonen wurden aufgrund von $P > 0,2$ aus dem endgültigen Modell ausgeschlossen, wenn HC und TC die abhängigen Variablen waren.*

Independent parameters	$T1_{PostGd}$ thickness (μm) (range)	P-value	$T2_{map}$ thickness (μm) (range)	P-value	TC thickness (μm) (range)	P-value	HC thickness (μm) (range)	P-value
Intercept		<0.001		<0.001		<0.001		<0.001
Normal cartilage	1253 (517–1791)	-						
Mild - moderate OA	1179 (516–1974)	0.444						
Severe OA	986 (519–2030)	0.039						
P2	1121 (521–1791)	0.189			1662 (969–3263)	<0.001	1477 (695–2961)	<0.001
P3	1244 (346–2030)	-			2127 (885–3165)	-	1992 (767–3035)	-
Dorsal	950 (516–1791)	-	1078 (468–1670)	-	1806 (1019–2590)	-	1571 (876–2307)	-
Central	1283 (346–2030)	<0.001	1112 (311–2177)	0.018	2089 (885–3165)	<0.001	1952 (787–2807)	<0.001
Palmar	1102 (532–1974)	0.007	1088 (590–1796)	0.95	1558 (969–3263)	0.495	1391 (695–3035)	0.757
Condyle			1037 (311–2177)	-				
Condylar groove			1162 (468–1944)	<0.001				

histological cartilage thickness (TC and HC) was not significantly different in the dorsal and palmar zone. When measuring on $T1_{PostGd}$ and $T2_{map}$ cartilage thickness in the dorsal zone of the DIPJ was also significantly less than in the central zone, and additionally was found less in the palmar zone. Cartilage thickness located on the condyles and in the condylar groove was not significantly different when measured histologically or on $T1_{postGd}$. However on measured on $T2_{map}$, the articular cartilage located on the condyles was significantly thinner than the cartilage located in the condylar groove.

When measured histologically distal P2 articular cartilage was significantly thinner than proximal P3 cartilage (Table 2). $T2_{map}$ and $T1_{postGd}$ cartilage thickness measurements did not detect this difference in cartilage thickness.

Discussion

To ensure that the cartilage surface and the bone-cartilage interface of dGEMRIC and T2 mapping sites are consistent with true anatomical sites, validation studies need to be performed to compare MRI cartilage thickness measurements to histological measurements as the gold standard. This was the goal of this study, where DIPJ cartilage thickness was measured on histological slices, dGEMRIC and T2 map of normal and osteoarthritic DIPJs, and the measurements were compared. Overall the measurements showed a positive correlation between histological measurements and MR measurements, whereby overall the articular cartilage was better identified on $T1_{PostGd}$ compared to $T2_{map}$. On $T1_{PostGd}$ the contrast between the hyperintense articular cartilage and the hypointense synovial fluid and the subchondral bone was high, whereas on $T2_{map}$ the intermediate intense cartilage only had low contrast compared to the hypointense subchondral bone. A similar finding was reported by *Olive et al*. when assessing the DIPJ cartilage in a low field MRI, where sagittal high-resolution T1-weighted gradient recalled echo images were best to evaluate full and partial cartilage erosions, due to the same reason (*Olive* 2010). Further $T1_{PostGd}$ detected that cartilage affected by OA was thinner than normal cartilage. This was not detected by $T2_{map}$. Cartilage thinning is one of the consequences of OA. Irrespective of the etiological factor of OA, it finally leads to thinning of the articular cartilage, especially in areas of high load. It was encouraging that in our study the inter observer agreement of MRI measurements was excellent in $T1_{PostGd}$ (ICC = 0.953) and optimal in $T2_{map}$ (ICC = 0.835). The mildly inferior ICC of $T2_{map}$ compared to $T1_{PostGd}$ may also be related to the above mentioned hypointense cartilage seen as a progressive continuum of the hypointense subchondral bone on $T2_{map}$.

In agreement with our hypothesis there were region dependent differences on the DIPJ cartilage thickness, which was anticipated, and is likely due to the differences of the joint inherent characteristic biomechanical loading. As an example: the dorsal zone of the DIPJ may undergo intermittent loading whereas the central and palmar zones of the joint are exposed to quite consistent loads. In agreement with this, this study showed that centrally within the DIPJ the cartilage was thickest and dorsally thinnest. This was detected by histological measurements and confirmed by $T1_{PostGd}$ and $T2_{map}$ measurements. This is also in agreement with *Olive* et al. (*Olive* 2010), who also described thickening of the palmarocentral region of the DIPJ, and a dorsal articular cartilage thinning in low field MRI. Similarly *Bischofberger et al*. (*Bischofberger* et al. 2018) found that cartilage zone and location within the DIPJ evaluated by dGEMRIC was significantly associated with the T1 pre gadolinium relaxation times. The dorsal zone of the DIPJ had significantly shorter median T1 relaxation times than the middle or palmar zones of the DIPJ, where cartilage relaxation times were longer and glycosaminoglycan production greater.

Histologically TC and HC thicknesses were not different when comparing the dorsal and the palmar zone. However, $T1_{PostGd}$ and $T2_{map}$ appreciated dorsal thinning of the articular cartilage compared to the palmar in this study. Similar, histologically TC and HC thickness were the same in the condylar and intercondylar groove region, however $T2_{map}$ appreciated a condylar cartilage thinning. Cartilage curvature is a very important factor. In the above mentioned regions within the DIPJ the articular cartilage curvature is greatest leading to volume averaging of articular cartilage and synovial fluid, and subsequent MR measurement inaccuracies. A similar problem has been described in the human knee, where it has been shown that the weight-bearing and central areas on each femoral and tibial condyle yielded more accurate measurements than boundary and non-weight-bearing regions based on sagittal plane MR imaging (*Koo* et al. 2005).

For the DIPJs evaluated histologically in the present study the proximal P3 TC and HC was thicker than the distal P2 cartilage, likely owing to continuous loading of the articular surface of P3 and the cartilage being thicker as adaption to these loads. A similar distribution was found when measuring T1 pre-gadolinium relaxation times in the DIPJ where relaxation times for the P3 articular surface were significantly greater than for the P2 articular surface. This difference in cartilage thickness was not depicted by $T1_{PostGd}$ and $T2_{map}$ in this study. The lack of detection of this finding may represent a true limitation of MRI for cartilage thickness measurement, however histological thickness measurements may also have been affected by the histological processing.

The DIPJs were obtained from horses of different ages. Therefore, the articular cartilage lesions observed were likely caused by a multitude of factors including age-related osteoarthritis and overload injuries. In the present study TC and HC thickness difference were not detected between the groups of cartilage health histologically. This may represent a pool of DIPJs not severely enough affected by naturally occurring osteoarthritis causing cartilage thinning, or it is possible that the differences in grades of osteoarthritis between the cartilage health groups was too subtle, or the sample size was too small to detect a significant difference.

Olive et al. (*Olive* 2010) and *Carstens* et al. (*Carstens* et al. 2013) reported that opposing cartilage plates of equine DIPJs and metacarpo/metatarsophalangeal joints could not be reliably separated on MR images, when the joint space was very narrow. This was most likely due to the use of a low-field magnet for the image acquisition in the study of *Olive et al*., which resulted in poorer image quality (*Olive* 2010). In the study of *Carstens et al*. (*Carstens* et al. 2013) a combination of the very thin articular cartilage (<1 mm) and partial volume

averaging of the thin intra-articular space were likely reasons for the poor differentiation in regions of opposing cartilage surfaces. To separate the two opposing cartilage surfaces in the human knee, the use of traction was described to improve the evaluation (*Trattnig* et al. 2008). This technique may also be considered in the future when evaluating opposing joint cartilages in the horse when performing MR under general anesthesia, especially when only a low field system is available and a cartilage lesion is suspected or when the articular cartilage is very thin. Likely using a 3 Tesla magnet and the fact that the DIPJ cartilage was slightly thicker as measured in the metacarpo/metatarsophalangeal joint omitted these problems in our study. Voxels were anisotropic and size ranged from 1.1–22 mm to 1.05–1.28 mm for dGEMRIC and T2 maps, respectively. Given the thin cartilage thickness at some sites, the voxel size and its anisotropic nature needs to be added as a limitation in this study and may have influenced measurement accuracy to a small degree.

It has been shown that dGEMRIC and T2 cartilage mapping are accurate techniques for measuring equine cartilage thickness at the distal third metacarpal/metatarsal bone (*Carstens* et al. 2013). The normal cartilage of the distal third metacarpal/metatarsal bone is approximately 1 mm thick (*Carstens* et al. 2013) versus the average thickness of the DIPJ cartilage in our study (Table 2) and 2.1–3.1 mm when measured on low field MR images (*Olive* 2010). The metacarpophalangeal joint has a more rounded articular surface compared to the DIPJ, so direct comparisons cannot be made. A high-field MRI ($\geq$ 1 tesla) is regarded as the modality of choice to evaluate the articular cartilage of horses, because a more appropriate method does not exist yet (*Pease* 2012). A human study comparing 3 tesla with 1.5 tesla images reported superior cartilage thickness measurements when using the higher field magnet strength (*Eckstein* et al. 2005). We used slice thicknesses of 2.5–3 mm. The use of thinner slices for MRI scans in our study would have resulted in a lower signal to noise ratio however would have required more scanning time. Findings in a study evaluating the human knee cartilage volume showed that there was only little difference in the human tibial cartilage volume when slice thicknesses were increased from 1.5 to 7.5 mm (*Cicuttini* et al. 2004). The DIPJ cannot directly be compared with the human knee, but it can be assumed that our slice thicknesses gave reliable results.

The present study had a few unavoidable limitations. Despite a template being used to match the location of the thickness measurements on the MRI images with the locations from which osteochondral core tissue specimens were obtained for the histological thickness measurements, small deviations may have occurred. To avoid this, the actual osteochondral core tissue specimens would have had to be scanned, histologically evaluated and the respective cartilage thickness measurements obtained. However, for this study, we chose to scan the entire DIPJ to more closely imitate a clinical situation. The fact that cadavers were used in the study may have had an impact on the absorption rate of the contrast agent in the cartilage, however did not affect $T1_{PostGd}$ cartilage thickness measurements notably.

Cartilage thickness measurements on $T1_{PostGd}$ and $T2_{map}$ compared to histology were reliable: there was an overall positive correlation between dGEMRIC and T2 mapping, and the histological cartilage thickness measurements in normal and severely osteoarthritic cartilage. There were regional differences in cartilage thickness depending on the cartilage site within the joint: the articular cartilage centrally within the DIPJ was thickest with thinning towards dorsally, reliably identified on both $T1_{PostGd}$ and $T2_{map}$. In regions of greatest cartilage curvature in the DIPJ volume averaging was likely the main limitation for MRI supporting histological measurements. Topographical variations of DIPJ cartilage thickness and volume averaging as a complicating factor should be appreciated by clinicians to avoid misinterpretation of cartilage thinning secondary to cartilage disease, especially in the joint periphery.

Acknowledgements

The authors thank Andrea Bachmann, Angela Kirchmeier and Muriel Federici for their help with the image analysis.

Conflict of interest statement and funding

The authors have no personal interests to declare. The study was funded by the Swiss Veterinary Association.

This manuscript represents a portion of a thesis submitted by Dr. *Bischofberger* to the Graduate School for Cellular and Biomedical Sciences, University of Bern, Switzerland, as partial fulfilment of the requirements for a Doctor of Philosophy degree.

References

Baker M. E., *Kershaw L. E.*, *Carstens A.*, *Daniel C. R.*, *Brown H.*, *Roberts S.*, *Taylor S. E.* (2022) T2 mapping of cartilage in the equine distal interphalangeal joint with corresponding histology using 0.27 T and 3.0 T magnetic resonance imaging. Equine Vet. J. 1–10; DOI 10.1111/evj.13900

Bekkers J. E. J., *Bartels L. W.*, *Benink R. J.*, *Tsuchida A. I.*, *Vincken K. L.*, *Dhert W. J. A.*, *Creemers L. B.*, *Saris D. B. F.* (2013) Delayed gadolinium enhanced MRI of cartilage (dGEMRIC) can be effectively applied for longitudinal cohort evaluation of articular cartilage regeneration. Osteoarthr. Cartil. 21, 943–949; DOI 10.1016/j.joca.2013.03.017

Bekkers J. E. J., *Creemers L. B.*, *Dhert W. J. A.*, *Saris D. B. F.* (2010) Diagnostic Modalities for Diseased Articular Cartilage-From Defect to Degeneration: A Review. Cartilage 1, 157–164; DOI 10.1007/s00330-017-5277-y

Bischofberger A. S., *Fürst A. E.*, *Torgerson P. R.*, *Carstens A.*, *Hilbe M.*, *Kircher P.* (2018) Use of a 3-Telsa magnet to perform delayed gadolinium-enhanced magnetic resonance imaging of the distal interphalangeal joint of horses with and without naturally occurring osteoarthritis. Am. J. Vet. Res. 79, 287–298; DOI 10.2460/ajvr.79.3.287

Carstens A., *Kirberger R. M.*, *Dahlberg L. E.*, *Prozesky L.*, *Fletcher L.*, *Lammentausta E.* (2013) Validation of Delayed Gadolinium-Enhanced Magnetic Resonance Imaging of Cartilage and T2 Mapping for Quantifying Distal Metacarpus/Metatarsus Cartilage Thickness in Thoroughbred Racehorses. Vet. Radiol. Ultrasound 54, 139–148; DOI 10.1111/vru.12002.

Carstens A., *Kirberger R. M.*, *Velleman M.*, *Dahlberg L. E.*, *Fletcher L.*, *Lammentausta E.* (2013) Feasibility for Mapping Cartilage T1 Relaxation Times in the Distal Metacarpus3/Metatarsus3 of Thoroughbred Racehorses Using Delayed Gadolinium-Enhanced Magnetic Resonance Imaging of Cartilage (Dgemric): Normal Cadaver Study. Vet. Radiol. Ultrasound 54, 365–372; DOI 10.1111/vru.12030

Choi J. A., *Gold G. E.* (2011) MR Imaging of Articular Cartilage Physiology. Magn. Reson. Imag. Clin. North Am. 19, 249–282; DOI 10.1016/j.mric.2011.02.010

Cicuttini F., *Morris K. F.*, *Glisson M.*, *Wluka A. E.* (2004) Slice thickness in the assessment of medial and lateral tibial cartilage volume and accuracy for the measurement of change in a longitudinal study. J. Rheumatol. 31, 2444–2448

Domayer S. E., *Welsch G. H.*, *Dorotka R.*, *Mamisch T. C.*, *Marlovits S.*, *Szomolanyi P.*, *Trattnig S.* (2008) MRI Monitoring of Cartilage Repair in the Knee: A Review. Sem. Musculoskelet. Radiol. 12, 302–317; DOI 10.1055/s-0028-1100638

Dyson S. J. (1991). Lameness Due to Pain Associated with the Distal Interphalangeal Joint - 45 Cases. Equine Vet. J. 23, 128–135; DOI 10.1111/j.2042-3306.1991.tb02737.x

Eckstein F., *Charles H. C.*, *Buck R. J.*, *Kraus V. B.*, *Remmers A. E.*, *Hudelmaier M.*, *Wirth W.*, *Evelhoch J. L.* (2005) Accuracy and precision of quantitative assessment of cartilage morphology by magnetic resonance imaging at 3.0T. Arthritis Rheum. 52, 3132–3136

Frisbie D. D. (2012). Synovial joint biology and pathobiology. Equine Surgery. J. S. J. Auer. St. Louis, Missouri, Elsevier, Saunders. 1096–1114; DOI 10.1016/B978–1-4377-0867-7.00078-8

Gold G. E., *Burstein D.*, *Dardzinski B.*, *Lang P.*, *Boada F.*, *Mosher T.* (2006) MRI of articular cartilage in OA: novel pulse sequences and compositional/functional markers. Osteoarthr. Cartilage 14, A76-A86; DOI 10.1016/j.joca.2006.03.010

Goodrich L. R., *Nixon A. J.* (2006) Medical treatment of osteoarthritis in the horse - A review. Vet. J. 171, 51–69; DOI 10.1016/j.tvjl.2004.07.008

Goodwin D. W. (2001) Visualization of the macroscopic structure of hyaline cartilage with MR imaging. Semin. Musculoskelet. Radiol. 5, 305–312; DOI 10.1055/s-2001-19041

Jeffcott L. B., *Rossdale P. D.*, *Freestone J.*, *Frank C. J.*, *Towersclark P. F.* (1982) An Assessment of Wastage in Thoroughbred Racing from Conception to 4 Years of Age. Equine Vet. J. 14, 185–198; DOI 10.1111/j.2042-3306.1982.tb02389.x

Koo S., *Gold G. E.*, *Andriacchi T. P.* (2005) Considerations in measuring cartilage thickness using MRI: factors influencing reproducibility and accuracy. Osteoarthr. Cartil. 13, 782–789; DOI 10.1016/j.joca.2005.04.013

Kristiansen K. K., *Kold S. E.* (2007) Multivariable analysis of factors influencing outcome of 2 treatment protocols in 128 cases of horses responding positively to intra-articular analgesia of the distal interphalangeal joint. Equine Vet. J. 39, 150–156; DOI 10.2746/042516407x170094

Lacourt M., *Gao C.*, *Li A.*, *Girard C.*, *Beauchamp G.*, *Henderson J. E.*, *Laverty S.* (2012) Relationship between cartilage and subchondral bone lesions in repetitive impact trauma-induced equine osteoarthritis. Osteoarthrit. Cartil. 20, 572–583; DOI 10.1016/j.joca.2012.02.004

Mankin H. J., *Dorfman H.*, *Lippiell L.*, *Zarins A.* (1971) Biochemical and Metabolic Abnormalities in Articular Cartilage from Osteo-Arthritic Human Hips .2. Correlation of Morphology with Biochemical and Metabolic Data. J. Bone Joint Surg. Am. Vol. A 53, 523–537

McKnight A. L., *Posh J.* (2012) Articular cartilage lesions seen with MRI at 0.25T in the distal equine limb. J. Equine Vet. Sci. 32, 667–671

Menendez M. I., *Clark D. J.*, *Carlton M.*, *Flanigan D. C.*, *Jia G.*, *Sammet S.*, *Weisbrode S. E.*, *Knopp M. V.*, *Bertone A. L.* (2011) Direct delayed human adenoviral BMP-2 or BMP-6 gene therapy for bone and cartilage regeneration in a pony osteochondral model. Osteoarthr. Cartilage 19, 1066–1075; DOI 10.1016/j.joca.2011.05.007

Mosher T. J., *Dardzinski B. J.* (2004) Cartilage MRI T2 relaxation time mapping: overview and applications. Sem. Musculoskelet. Radiol. 8, 355–368; DOI 10.1055/s-2004-861764

Nelson B. B., *Stewart R. C.*, *Kawcak C. E.*, *Freedman J. D.*, *Patwa A. N.*, *Snyder B. D.*, *Goodrich L. R.*, *Grinstaff M. W.* (2021) Quantitative Evaluation of Equine Articular Cartilage Using Cationic Contrast-Enhanced Computed Tomography. Cartilage 12, 211–221; DOI 10.1177/1947603518812562

Olive J. (2010) Distal interphalangeal articular cartilage assessment using low-field magnetic resonance imaging. Vet. Radiol. Ultrasound 51, 259–266; DOI 10.1111/j.1740-8261.2009.01663.x

Olive J., *D'*Anjou *M. A.*, *Girard C.*, *Laverty S.*, *Theoret C.* (2010) Fat-suppressed spoiled gradient-recalled imaging of equine metacarpophalangeal articular cartilage. Vet. Radiol. Ultrasound 51, 107–115; DOI 10.1111/j.1740-8261.2009.01633.x

Pease A. (2012) Biochemical Evaluation of Equine Articular Cartilage Through Imaging. Vet. Clin. North Am. Equine Pract. 28, 637–46; DOI10.1016/j.cveq.2012.08.004

Potter H. G., *Black B. R.*, *Chong L. R.* (2009) New Techniques in Articular Cartilage Imaging. Clin. Sports Med. 28, 77–94; DOI 10.1016/j.csm.2008.08.004

Trattnig S., *Mamisch T. C.*, *Pinker K.*, *Domayer S.*, *Szomolanyi P.*, *Marlovits S.*, *Kutscha-Lissberg F.*, *Welsch G. H.* (2008) Differentiating normal hyaline cartilage from post-surgical repair tissue using fast gradient echo imaging in delayed gadolinium-enhanced MRI (dGEMRIC) at 3 Tesla. Europ. Radiol. 18, 1251–1259; DOI 10.1007/s00330-008-0859-3

Trattnig S., *Marlovits S.*, *Gebetsroither S.*, *Szomolanyi P.*, *Welsch G. H.*, *Salomonowitz E.*, *Watanabe A.*, *Deimling M.*, *Mamisch T. C.* (2007) Three-dimensional delayed gadolinium-enhanced MRI of cartilage (dGEMRIC) for in vivo evaluation of reparative cartilage after matrix-associated autologous chondrocyte transplantation at 3.0T: Preliminary results. J. Magnet. Reson. Imag. 26, 974–982; DOI 10.1002/jmri.21091

Trattnig S., *Mlynarik V.*, *Breitenseher M.*, *Huber M.*, *Zembsch A.*, *Rand T.*, *Imhof H.* (1999) MRI visualization of proteoglycan depletion in articular cartilage via intravenous administration of Gd-DTPA. Magn. Reson. Imag. 17, 577–583; DOI 10.1016/s0730-725x(98)00215-x

Xia Y., *Moody J. B.*, *Alhadlaq H.* (2002) Orientational dependence of T2 relaxation in articular cartilage: A microscopic MRI (microMRI) study. Magn. Reson. Med. 48, 460–469; DOI 10.1002/mrm.10216